ELSEVIER

# Self-assembly of ABC coil-rod-coil triblock molecules with perforated lamellar mesophases

Nam-Keun Oh [a], Wang-Cheol Zin [a,*], Jun-Hwan Im [b], Myongsoo Lee [b,**]

[a] *Department of Materials Science and Engineering, Polymer Research Institute, Pohang University of Science and Technology, Pohang 790-784, South Korea*
[b] *Center for Supramolecular Nano-Assembly and Department of Chemistry, Yonsei University, Shinchon 134, Seoul 120-749, South Korea*

## Abstract

The synthesis and characterization of ABC coil-rod-coil triblock (monomer) and ABCBA coil-rod-coil-rod-coil triblock dimer (dimer) molecules of docosyl 4′-[4′-[methyloxypoly(ethyleneoxy)ethyloxy]-4-biphenylcarboxyloxy]-4-biphenyl carboxylate with poly(ethylene oxide) (PEO) coil are described. The self-assembling behavior of triblock molecules is characterized by a combination of techniques consisting of differential scanning calorimetry (DSC), thermal polarized optical microscopy (POM), and X-ray diffraction (XRD) measurement. Monomer and dimer self-assemble into three lamellar crystalline phases ($k_1$, $k_2$, and $k_3$) and 3D-hexagonally perforated lamellar (HPL) and 2D-hexagonal columnar (col) liquid crystalline phases as temperature increases. In addition to the phases exhibited by monomer, dimer shows 3D-tetragonally perforated lamellar (TPL) and spherical micellar (M) liquid crystalline phases. These results demonstrate that simple dimerization of coil-rod-coil molecule by connecting PEO block induces 3D-tetragonally perforated lamellar and spherical micellar mesophases.
© 2006 Elsevier Ltd. All rights reserved.

*Keywords:* ABCBA coil-rod-coil-rod-coil triblock dimer molecule; Dimerization; 3D-Tetragonally perforated lamellar liquid crystalline phase

## 1. Introduction

The development of novel functional materials based on self-assembling systems has a great deal of attention due to their potential in the well-defined supramolecular nanostructures [1]. An example of a self-assembling system is provided by rod-coil molecules, which have a strong tendency to self-organize into a variety of supramolecular structures in nano-scale dimensions [2]. Supramolecular architectures of rod-coil molecules can self-assemble into a rich variety of nanoscale structures through a combination of shape complementarity and repulsive interaction between rigid and flexible parts. Apart from the wide range of different supramolecular structures in nano-scale dimensions, another unique characteristic is that rod segments can endow various functionalities to supramolecular materials, such as photophysical and electrochemical properties [3].

We have previously shown that ABC coil-rod-coil triblock molecules self-assemble into various supramolecular

architectures such as layered lamellar, hexagonal columnar, and spherical micellar liquid crystalline phase depending on the coil volume fraction in the molecules [4]. The triblock molecules have a lamellar ABCCBAA···stacking sequence in the crystalline phase. However, there may be a small possibility of stacking fault such as an ABCABCA···stacking sequence. A strategy for elaborate manipulation of various well-defined supramolcular nanostructures may be accessed by binding the C coil block of ABC coil-rod-coil triblock molecule. This binding may slightly modify the entropic contribution of the C coil part in the ABC coil-rod-coil system. Also, the elimination of stacking fault supplies the driving force to form well-defined nanostructures. In a preliminary communication, we demonstrated that tetra-branched ABC coil-rod-coil triblock molecule induces an unusual tetragonally perforated lamellar mesophase as an intermediate structure between lamellar and hexagonal columnar phase [5]. But, the attachment of four coils into a central point has the strong effect of reducing the freedom of movement for the flexible chains. In comparison with tetramer, dimer has the weak restriction of chain end mobility. The elimination of stacking fault through covalent linkage and this weak restriction may bring about the formation of various well-defined supramolecular nanosturcture. With this idea in mind, we have synthesized ABC coil-rod-coil triblock molecule (designated as monomer) and ABCBA coil-rod-coil-rod-coil

* Corresponding authors. Fax: +82 54 279 2399.
** Fax: +82 2 393 6096.
*E-mail addresses:* wczin@postech.ac.kr (W.-C. Zin), mslee@yonsei.ac.kr (M. Lee).

triblock dimer molecule (designated as dimer) with specific coil volume fraction. Momomer and dimer consist of docosyl (designated as PE) chain as an A block, a molecular rod (designated as rod) containing two biphenyl units connected through ester linkages as a B block, and poly(ethylene oxide) (designated as PEO) as a C block (Fig. 1).

We report here on the synthesis of triblock molecules and these self-organization behaviors characterized by polarized optical microscopy (POM), differential scanning calorimetry (DSC), and X-ray diffraction (XRD) measurements. Various well-defined supramolecular nanostructures induced through simple binding of coil block will be demonstrated.

## 2. Experimental

### 2.1. Materials and measurements

$4'$-Hydroxy-4-biphenyl carboxylic acid (98%), toluene-$p$-sulfonyl chloride (98%) and 1-bromodocosane (95%) from Tokyo Kasei were used as received. Poly(ethylene glycol)s of DP = 17 and 34 (from Aldrich) and the other conventional reagents were used as received. $^1$H NMR spectra were recorded from CDCl$_3$ solutions on a Bruker AM 250 spectrometer. The purity of the products was checked by thin layer chromatography (TLC; Merck, silica gel 60). A Perkin–Elmer DSC-7 differential scanning calorimeter equipped with a 1020 thermal analysis controller was used to determine thermal transitions, which were reported as the maxima and minima of their endothermic or exothermic peaks. In all cases, heating and cooling rates were 10 °C min$^{-1}$. A Nikon Optiphot 2-pol optical polarized microscopy (magnification: 100×) equipped with a Mettler FP 82 hot-stage and a Mettler FP 90 central processor was used to observe the thermal transitions and to analyze anisotropic texture. Microanalyses were performed with a Perkin–Elmer 240 elemental analyzer at the Organic Chemistry Research Center. X-ray scattering measurements were performed in transmission mode with synchrotron radiation at the 3C2 and 4C1 X-ray beam line at the Pohang Accelerator Laboratory, South Korea. In order to investigate structural changes on heating, the sample was held in an aluminum sample holder, which was sealed with a window of 7 μm thick Kapton films on both sides. The sample was heated

with two cartridge heaters and the sample temperature was monitored by a thermocouple placed close to the sample. Background scattering correction was attained by subtracting the scatterings from the Kapton. Molecular weight distributions ($\bar{M}_w/\bar{M}_n$) were determined by gel permeation chromatography (GPC) with a Waters R401 instrument equipped with Stragel HR 3, 4 and 4E columns, M7725i manual injector, column heating chamber and 2010 Millennium data station. Measurements were made by using a UV detector, with CHCl$_3$ as solvent (1.0 mL min$^{-1}$). Molecular density ($\rho$) measurements were performed in an aqueous sodium chloride solution at 25 °C. The molecular length was calculated using Materials Studio Software.

### 2.2. Synthesis

Monomer synthesis has been performed by a produre similar to that previously described [6] and dimer was synthesized as outlined in Scheme 1.

Purified poly(ethylene oxide) with degrees of polymerization of 33 was used as a starting material for dimeric molecule. The poly(ethylene oxide) reacted with excess $p$-toluenesulfonyl chloride to yield compound 1. The substitution reaction of 1-bromodocosane with ethyl 4-hydroxy-4$'$-biphenyl carboxylic acid produced compound 2. The substitution reaction of compound 1 with ethyl 4-hydroxy-4$'$-bipheneyl carboxylated produced an intermediate, which was further hydrolyzed to yield compound 3. Compound 4 (dimer) was obtained by esterfication (25 °C, 24 h) 3 with 2 in CH$_2$Cl$_2$ in the presence of diisopropylcarbodiimide (DIPC) and 4-(dimethylamino)pyridinium-$p$-tolunene sulfonate (DPTS). The resulting dimer was purified by column chromatography (silica gel) using methylene chloride and methanol (8:1) as eluent until transition temperatures remained constant. It is well known that polydispersity influenced polymer phase behavior, especially those polymers with low molecular weight [7]. Therefore, it is essential that the rod-coil molecule is highly monodisperse to investigate its accurate phase behavior. As shown in Fig. 2, the MALDI-TOF mass spectra of dimer exhibit two signals, which can be as the K$^+$- and Na$^+$-molecular ions. The experimental mass based on the peak
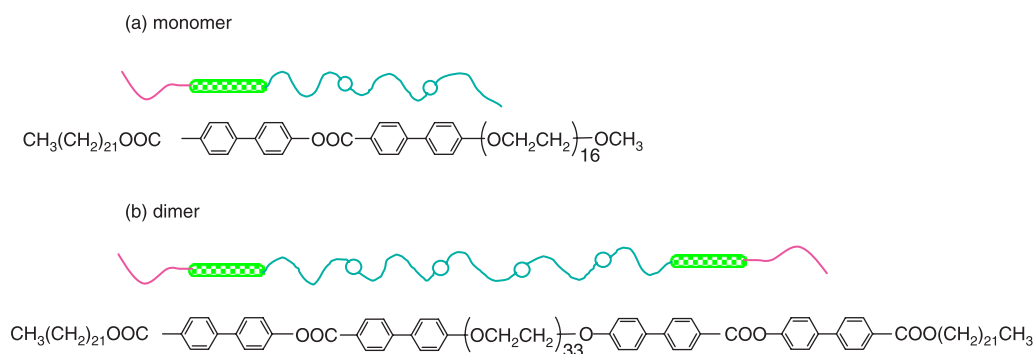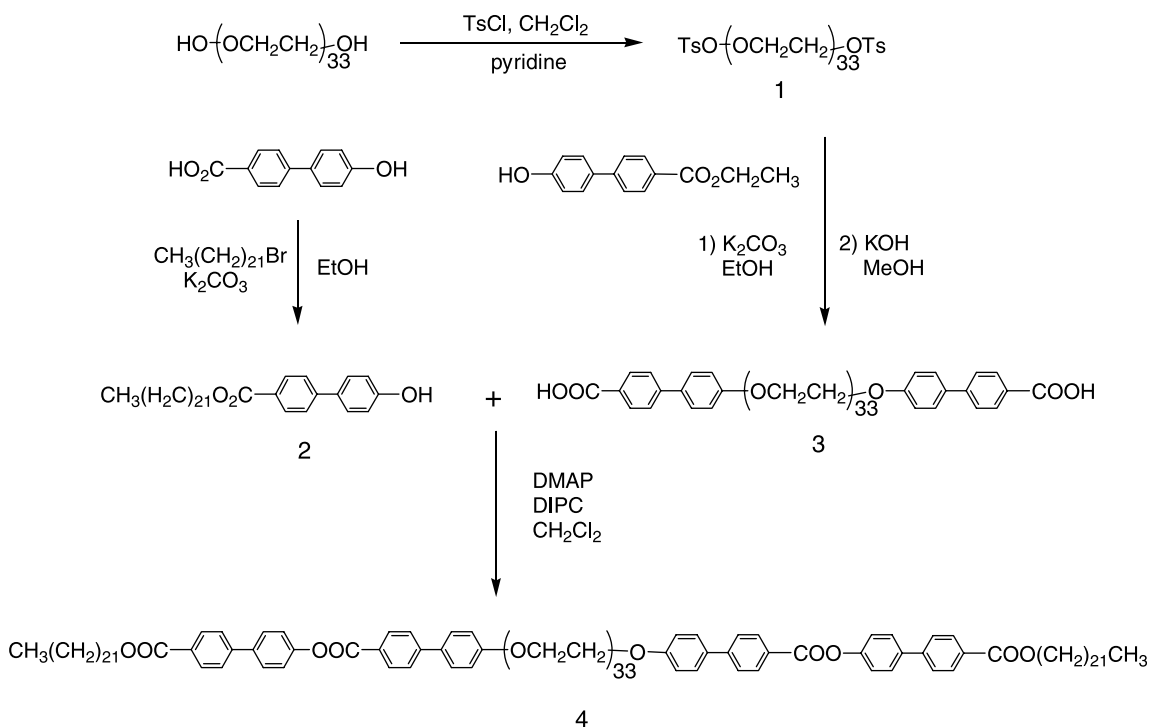


Fig. 1. Chemical structure and schematic drawings of coil-rod-coil triblock molecules (a) ABC monomer and (b) ABCBA dimer (PE/Rod/PEO (21.5/27.3/50.2 wt%)).

Scheme 1. Synthesis of ABCBA triblock dimer molecule (dimer).

positions in the spectrum is well matched with the theoretical molecular weight of each of dimer.

Synthesized monomer and dimer show a narrow molecular weight distribution with polydispersity index at a range of 1.02 and 1.03, as determined from gel permeation chromatography (GPC) relative to polystyrene standards, indicative of high purity. The product was characterized by ^{1}H NMR and elemental analysis. As confirmed by ^{1}H NMR spectroscopy, the number of repeating units in poly(ethylene oxide) coils of molecules determined from the ratio of aromatic protons (ortho to alkoxy) to the ethylene protons of poly(ethylene oxide) was in good agreement with the expected value.

### 2.2.1. Synthesis of poly(ethylene oxy) ethyl ditosylate (1)

Poly(ethylene glycol) (10 g, 0.011 mol) was dissolved in 30 mL of dry pyridine under argon. A solution of p-toluene-sulfonyl chloride (21 g, 0.11 mol) was dissolved in dry methylene chloride and then added dropwise to the mixture. The reaction mixture was stirred overnight at room temperature under argon. The resulting solution was poured into water and extracted with methylene chloride. The methylene chloride solution was washed with water, dried over anhydrous magnesium sulfate, and filtered. The solvent was removed in a rotary evaporator, and the crude product was purified by flash column chromatography (silica gel, methylene chloride: methanol (8:1) eluent) to yield 9.5 g (70.7%) of colorless oil.

1. Yield 70.7%; ^{1}H NMR (250 MHz, CDCl$_3$, $\delta$, ppm) 7.79 (d, 4Ar-H, $o$ to SO$_3$, $J = 7.5$ Hz), 7.34 (d, 4Ar-$H$, $o$ to CH$_3$, $J = 7.6$ Hz), 3.54–4.11 (m, 151H, OCH$_2$), 2.44 (s, 6H, C$H_3$ phenyl).

### 2.2.2. Synthesis of dococyl 4'-hydroxy-4-biphenyl carboxylate (2)

4'-Hydroxy-4-biphenyl carboxylic acid (2 g, 9.33 mmol), 1-bromodocosane (2.8 g, 7.18 mmol), and K$_2$CO$_3$ (0.64 g, 4.63 mmol) were dissolved in dry 100 mL ethanol. The mixture was heated at reflux for 50 h under nitrogen, and then cooled to room temperature. The solvent was removed in a rotary evaporator, the resulting mixture was poured into water and extracted with methylene chloride. The methylene chloride was washed with water, dried over anhydrous magnesium sulfate, and filtered. The solvent was removed in a rotary evaporator and the crude product was then purified by
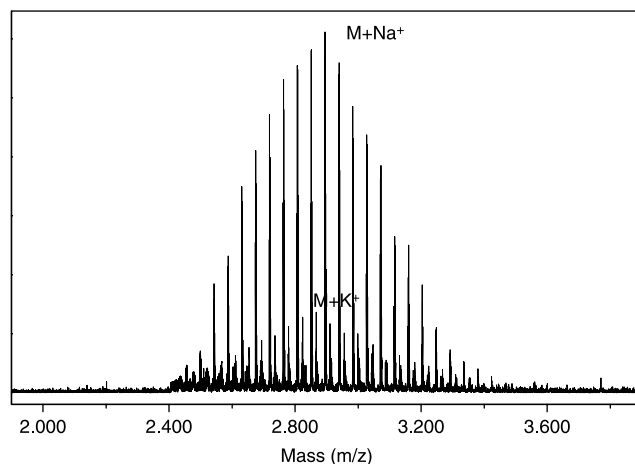


Fig. 2. MALDI-TOF mass spectra of dimer, showing the expected distribution for the PEO chain.

recrystallization from a mixture of methanol and hexane to yield 3.0 g (60%) of a white solid.

2. Yield 60%; ^{1}H NMR (250 MHz, CDCl$_3$, $\delta$, ppm) 8.06 (d, 2Ar-$H$, $o$ to COO, $J = 8.3$ Hz), 7.62 (d, 2Ar-$H$, $m$ to COO, $J = 8.3$ Hz), 7.53 (d, 2Ar-$H$, $m$ to OH, $J = 8.3$ Hz), 6.95 (d, 2Ar-$H$, $o$ to OH $J = 8.3$ Hz), 4.35 (t, 2H, CH$_3$(CH$_2$)$_{20}$C$H_2$,



J = 6.6 Hz), 1.77 (m, 2H, CH$_3$(CH$_2$)$_{19}$C$H_2$), 1.24–1.47 (m, 38H, CH$_3$(C$H_2$)$_{19}$), 0.87 (t, 3H, C$H_3$(CH$_2$)$_{21}$, $J = 6.8$ Hz). Elemental analysis for C$_{35}$H$_{54}$O$_3$, Calcd: C, 80.41; H, 10.41. Found: C, 80.57; H, 10.37.

### 2.2.3. Synthesis of 4′-[methyloxypoly(ethyleneoxy)ethyloxy]-4-biphenyl carboxylic acid (3)

Ethyl 4-hydroxy-4-biphenyl carboxylate (4 g, 0.01 mol) and K$_2$CO$_3$ (13.82 g, 0.1 mol) were dissolved in absolute ethanol 100 mL. The mixture was heated at reflux for 1 h, and compound 3 (10 g, 0.01 mmol) was added dropwise. The resulting solution was heated at reflux for 24 h, and then cooled to room temperature, and excess KOH was added. The mixture solution was stirred at room temperature for 12 h. The resulting solution was poured into water and extracted with methylene chloride. The methylene chloride was washed with water, dried over anhydrous magnesium sulfate, and filtered. The solvent was removed in a rotary evaporator and the crude product was then purified by flash column chromatography [silica gel, ethyl acetate and methylene chloride:methanol (8:1) eluent] to yield 3.4 g (47%) of a white waxy solid.

3. Yield 47%; ^{1}H NMR (250 MHz, CDCl$_3$, $\delta$, ppm) 8.11 (d, 4Ar-$H$, $o$ to COOH, $J = 7.6$ Hz), 7.63 (d, 4Ar-$H$, $m$ to COOH, $J = 7.6$ Hz), 7.55 (d, 4Ar-$H$, $m$ to CH$_2$O, $J = 7.5$ Hz), 6.98 (d, 4Ar-$H$, $o$ to CH$_2$O, $J = 10$ Hz), 3.50–4.20 (m, 130H, OC$H_2$). Elemental analysis for C$_{90}$H$_{146}$O$_{37}$, Calcd: C, 59.39; H, 8.09. Found: C, 59.47; H, 8.05, $M_n/M_w = 1.03$, mp 59–60 °C.

### 2.2.4. Synthesis of docosyl 4′-[4′-[methyloxypoly (ethyleneoxy)ethyloxy]-4-biphenylcarboxyl-oxy]-4-biphenyl carboxylate (4)

Compound 3 (2 g, 2.68 mmol), compound 2 (1.81 g, 3.5 mmol), and 4-dimethylaminopyridine (DMAP) (0.32 g, 2.68 mmol) were dissolved in 50 ml of dry methylene chloride under argon. The resulting mixture was stirred for 1 h and diisopropylcarbodiimide (DIPC) (0.5 ml, 0.13 mol) was stirred overnight at room temperature and then poured into methanol, the resulting precipitate purified by flash column
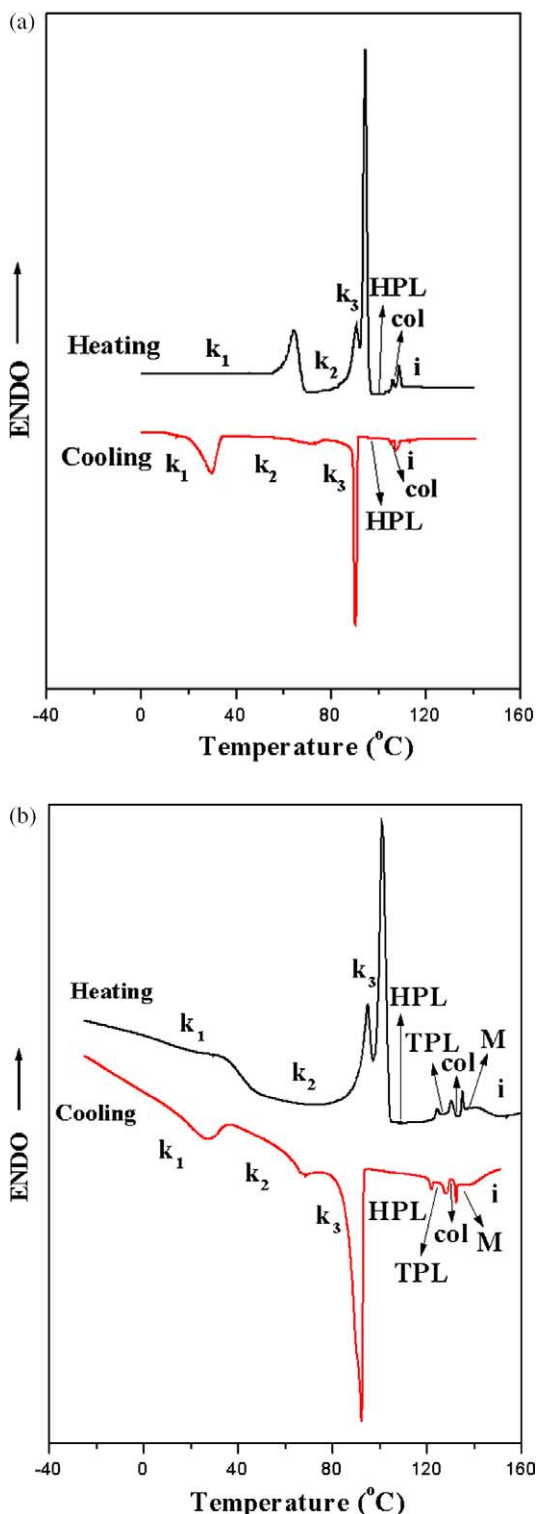
Fig. 3. DSC traces (10 °C/min) exhibited during second heating and first cooling scans by (a) monomer and (b) dimer.

Table 1
Thermal transitions of monomer and dimer molecules

| Molecule | Phase transitions (°C) and corresponding enthalpy changes (kJ/mol) | |
|---|---|---|
| | Heating | Cooling |
| Monomer | k$_1$65.4 (17.2)k$_2$90.4(3.6)k$_3$94.6 (56.4)HPL106.7(0.4) col109.2(3.9)I | i108.6(3.7)co104.8(0.4) HPL89.9(41.7)k$_3$70.6 (2.3)k$_2$29.3(54.3)k$_1$ |
| Dimer | k$_1$34.1 (38.9)k$_2$94.8 (13.2)k$_3$101(59.9)HPL124.2 (0.9)TPL130.3(1.7)col135 (1.5)M141.3(1.7)i | i 139.3 (2.9)M132.3 (1.2)col128.2(2)TPL122 (0.9)HPL92.2(94.3)k$_3$66.2 (8.4)k$_2$26.4(22.9)k$_1$ |

Data are from second heating and first cooling scans. k$_1$, first crystalline; k$_2$, second crystalline; k$_3$, third crystalline; HPL, hexagonally perforated lamellar; TPL, tetragonally perforated lamellar; col, hexagonal columnar; M, spherical micellar; i, isotropic.

chromatography [silica gel, eluent; methylene chloride and methanol (8:1) eluent] to yield 0.93 g (28%) of a white solid.

4. Yield: 28% ^{1}H NMR (250 MHz, CDCl$_3$, δ, ppm) 8.25 (d, 2Ar-*H*, *o* to COOphenyl, *J* = 7.5 Hz), 8.12 (d, 2Ar-*H*, *o* to COOCH$_2$, *J* = 10 Hz), 7.65–7.72 (m, 6Ar-*H*, *m* to COOphenyl, *m* to biphenylcarboxylate and *m* to COOCH$_2$), 7.60 (d, 2Ar-*H*, *m* to CH$_3$O, *J* = 7.5 Hz), 7.33 (d, 2Ar-*H*, *o* to biphenylcarboxylate, *J* = 7.5 Hz), 7.03 (d, 2Ar-*H*, *o* to CH$_2$O, *J* = 10 Hz), 4.32 (t, 2H, CH$_3$(CH$_2$)$_{20}$C*H$_2$*, *J* = 7.5 Hz) 4.19 (t, 2H, CH$_2$*CH$_2$*O-phenyl, *J* = 7.5 Hz), 3.89 (t, 2H, *CH$_2$*CH$_2$O-phenyl, *J* = 7.5 Hz), 3.52–3.74 (m, 44H, OCH$_2$), 3.37 (s, 3H, *CH$_3$*O), 1.77 (t, 2H, CH$_3$(CH$_2$)$_{19}$C*H$_2$*, *J* = 10 Hz), 1.18–1.47 (m, 38H, CH$_3$(*CH$_2$*)$_{19}$CH$_2$), 0.85 (t, 3H, *CH$_3$*(CH$_2$)$_{21}$, *J* = 7.5 Hz). Elemental analysis for C$_{160}$H$_{250}$O$_{41}$, Calcd: C, 67.91; H, 8.91. Found: C, 67.95; H, 8.89, $M_n/M_w$ = 1.03.
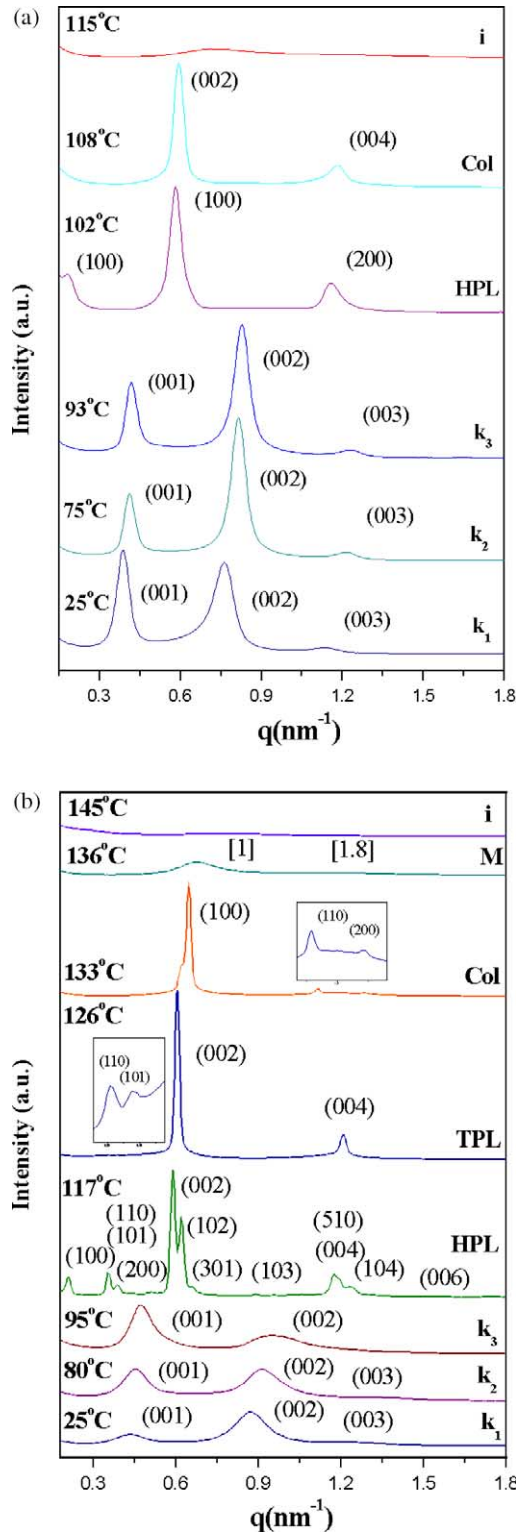


Fig. 4. Small-angle XRD patterns of (a) monomer and (b) dimer measured at various temperatures.
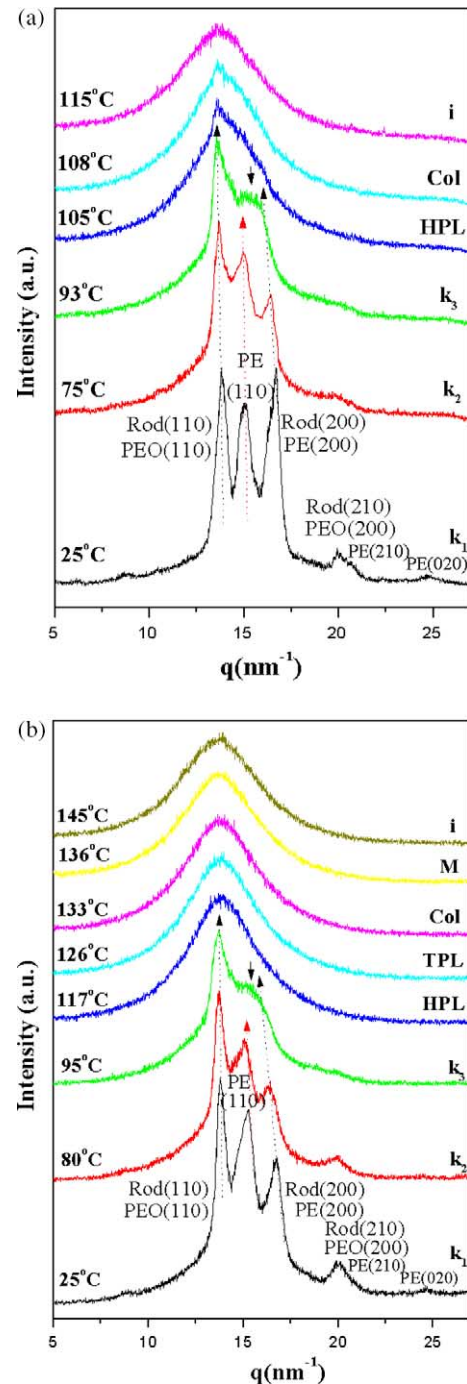


Fig. 5. Wide-angle XRD patterns of (a) monomer and (b) dimer measured at various temperatures.

Table 2
Characterization of monomer and dimer by small-angle XRD

| Molecule | Crystalline phase | | | Liquid crystalline phase | | | | | | | | | | | | | | | |
| --- | --- | --- | --- | --- | --- | --- | --- | --- | --- | --- | --- | --- | --- | --- | --- | --- | --- | --- | --- |
| | Lamellar | | | Hexagonally perforated lamellar | | | | | | Tetragonally perforated lamellar | | | | | | Hexagonal columnar | | Spherical micellar | |
| | First (k₁) | Second (k₂) | Third (k₃) | $d_{100}$ (nm) | $d_{002}$ (nm) | Lattice constant $a$ (nm) | $c$ (nm) | Perforation diameter $d$ (nm) | Wall thickness $W$ (nm) | $d_{110}$ (nm) | $d_{002}$ (nm) | Lattice constant $a$ (nm) | $c$ (nm) | Perforation diameter $d$ (nm) | Wall thickness $W$ (nm) | $d_{100}$ (nm) | Lattice constant $a$ (nm) | Primary peak (nm) | Diameter $d$ (nm) |
| | $d_{001}$ $d$ (nm) | | | | | | | | | | | | | | | | | | |
| Monomer | 16.2 | 15.3 | 15.0 | 34.3 | 10.8 | 39.6 | 21.6 | 26.7 | 13.0 | 17.8 | 10.3 | 25.1 | 20.7 | 18.6 | 6.5 | 10.6 | 12.2 | | |
| Dimer | 14.4 | 13.9 | 13.3 | 29.8 | 10.6 | 34.4 | 21.3 | 23.4 | 11.0 | | | | | | | 9.8 | 11.3 | 9.3 | 11.4 |

## 3. Results and discussion

### 3.1. Thermal characterization

The self-assembling behavior of molecules was investigated by differential scanning calorimetry (DSC), thermal polarized optical microscopy (POM), and X-ray diffraction (XRD) measurements. Fig. 3 presents DSC heating and cooling traces of monomer and dimer. The transition temperatures and corresponding enthalpy changes are summarized in Table 1.

As observed from Fig. 3, monomer and dimer exhibit three crystalline phases, respectively. In comparison with monomer, as seen in Fig. 3 and Table 1, the temperature range and thermal stability of mesophase in dimer increases. The crystalline melting temperature of PE (from $k_2$ to $k_3$) and rod block (from $k_3$ to HPL) in dimer is slightly higher than that of monomer. But the crystalline melting temperature of PEO block (from $k_1$ to $k_2$) in dimer is lower than that of monomer.

### 3.2. XRD studies of crystalline phases

To investigate the supramolecular nanostructures of monomer and dimer, small- and wide-angle XRD experiments were performed by increasing temperature in crystalline, liquid crystalline, and liquid phases, as shown in Figs. 4 and 5.

In the crystalline state, monomer and dimer show three crystalline melting transitions associated with PEO, PE, and Rod block, respectively. Monomer and dimer XRD patterns in the first crystalline phase (designated as $k_1$) display three reflections in the 1:2:3 spacing ratio in the small-angle region, while a number of sharp reflections are observed in the wide-angle region, indicative of a lamellar crystalline structure. The monomer and dimer layer distances are 16.2 and 14.4 nm, respectively. The monomer length in its most extended conformation is 9.5 nm, thus monomer is a bilayered lamellar structure, which is similar to dimer with the ABCBAA⋯stacking sequence in the crystalline phase. The layer distance measured at each crystalline phase for triblock molecules is summarized in Table 2.

The wide-angle XRD patterns in $k_1$ of monomer and dimer show a number of sharp reflections, indicating microphase-separated crystalline PE, rod and PEO domain as shown in Fig. 5. The flexible hydrophilic PEO and hydrophobic PE coil blocks and the stiff rod blocks are believed to be highly incompatible. Therefore, microphase separation will occur at each block, although the molecular weight of each block is very low. On the basis of wide-angle XRD measurements, lattice parameters $a^0$ and $b^0$ of each block unit cell in triblock molecule are obtained. The rod in $k_1$ is packed into a 2D-rectangular lattice with $a^0 = 7.5$ Å and $b^0 = 5.7$ Å. The PE chain domain in $k_1$ is also an rectangular lattice with $a^0 = 7.5$ Å and $b^0 = 5.0$ Å as summarized in Table 3.

The lattice parameters of PE chain in triblock molecule are similar to those of pure PE, which is packed into a rectangular lattice with $a^0 = 7.4$ Å and $b^0 = 4.9$ Å [8]. The density ($\rho$) of each block can be calculated from the volume and molecular weight in each block. The density of PE chain in triblock

Table 3
Characterization of monomer and dimer by wide-angle XRD

| Lamellar crystalline phase | | | | | | | | |
|---|---|---|---|---|---|---|---|---|
| Molecule | Block | First ($k_1$) | | Second ($k_2$) | | Third ($k_3$) | | |
| | | Lattice constant | | Lattice constant | | Lattice constant | | |
| | | $a^0$ (Å) | $b^0$ (Å) | $a^0$ (Å) | $b^0$ (Å) | $a^0$ (Å) | $b^0$ (Å) | |
| Monomer | PE | 7.5 | 5.0 | 7.7 | 5.0 | | | |
| | Rod | 7.5 | 5.7 | 7.7 | 5.7 | 7.9 | 5.7 | |
| | PEO | 6.4 | 6.6 | | | | | |
| Dimer | PE | 7.5 | 5.0 | 7.7 | 5.0 | | | |
| | Rod | 7.5 | 5.7 | 7.7 | 5.7 | 7.9 | 5.7 | |
| | PEO | 6.4 | 6.6 | | | | | |

molecule is equal to that of pure PE, which is $\rho = 1.00$ g/cm$^3$ in $k_1$. The PEO chain in $k_1$ is packed into a rectangular lattice with $a^0 = 6.4$ Å and $b^0 = 6.6$ Å. The pure PEO crystal is monoclinic with chains in 7/2 helical conformations [9]. Its unit cell parameters are $a = 8.1$ Å, $b = 13.0$ Å ($\approx 2a \sin \beta$), $\beta = 125.4°$, and $N = 4$; the projection of the unit cell onto the plane normal to the chain axis is a 2D-rectangular lattice with $a^0 = 6.6$ Å, $b^0 = 6.5$ Å, and $N = 2$. Lattice parameters of PEO chain in triblock molecule are nearly similar to those of pure PEO.

In order to form lamellar crystalline structure, the cross-section area of each block should be the same. On the basis of the reduced layer distance on heating, schematic representations of packing structural behavior in each lamellar crystal can be constructed as shown in Fig. 6.

These indicate that PEO crystalline chain melts as the phase changes from $k_1$ to $k_2$, and the degree of tilting of rod increases, thus layer distance decreases. During the change from $k_2$ to $k_3$, PE crystalline chain melts, and rod tilt increases, therefore, layer distance decreases further. In comparison with monomer, dimer shows higher tilting of rod in order to reduce the entropy loss associated with stretching of PEO chain.
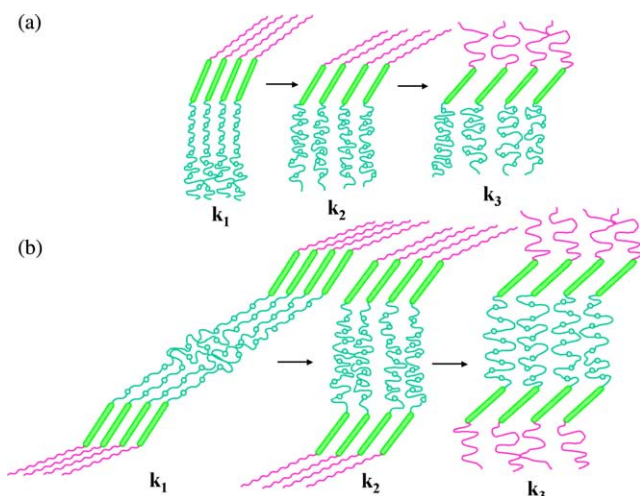
### 3.3. POM studies of liquid crystalline phases

Monomer and dimer show enantiotropic mesophase behavior, as revealed by DSC and POM.

On cooling from isotropic liquid at 145 °C, a pseudo-focal-conic texture of dimer was observed at 132 °C as shown in Fig. 7, which is characteristic of the hexagonal columnar mesophase exhibited by conventional discotic mesogens [10]. Monomer can also be observed with pseudo-focal-conic texture at 106 °C. On cooling from the hexagonal columnar mesophase in dimer, isotropic areas with curved edges appear on pesudo-focal-conic domains and these regions then grow until the entire field of view darkens, which maybe tetragonally perforated lamellar (TPL) mesophase at 127 °C. Monomer also exhibits isotropic texture, which maybe hexagonally perforated lamellar (HPL) mesophase at 103 °C. On further cooling from the TPL mesophase in dimer, optically isotropic texture does not change until 93 °C. These results indicate that rod segments aligned axially normal to the micrograph plane with long-range order extending over areas, such as smectic A ($S_A$) mesophase with homeotropic texture [11]. Upon heating from hexagonal columnar mesophase, dimer exhibits optically isotropic mesophase at 135 °C. DSC measurement indicated the presence of an additional phase transition. This transition can also be detected microscopically by a significant increase in fluidity. Considering thermal behavior, which exhibits an intermediate phase between the columnar liquid crystalline and isotropic liquid phases, the optically isotropic phase is considered as a spherical micellar phase [4].

### 3.4. XRD studies of liquid crystalline phases

To confirm the mesophase determined from optical microscopic observations, XRD experiments have been performed with increasing temperatures (Figs. 4 and 5). In the mesophase, a diffuse halo was observed in the wide-angle region, indicating a lack of any positional long-range order of rod segments (Fig. 5).
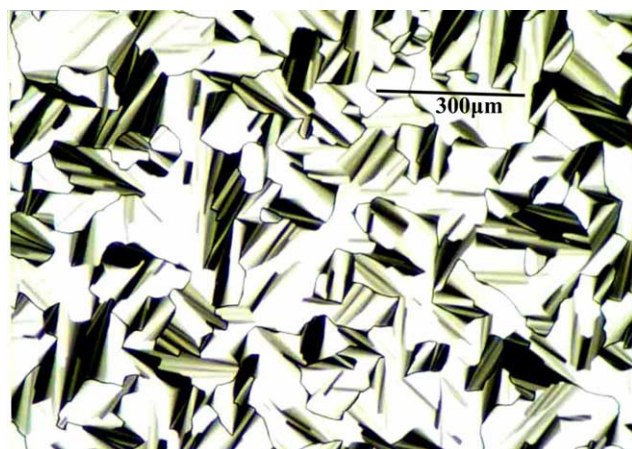


Fig. 6. Packing structural behavior of (a) monomer and (b) dimer in lamellar crystalline phases.



Fig. 7. Representative polarized optical micrographs (100×) of dimer textures exhibited by hexagonal columnar mesophase at 132 °C on the cooling scan.

The small angle XRD patterns of dimer at 117 °C show a number of well-resolved reflections, which indicate the existence of a highly ordered structure as shown in Fig. 8.

On the basis of results obtained from small angle XRD measurements, these reflections of dimer are indexed as a 3D hexagonally perforated lamellar (HPL) mesophase with lattice parameters $a = 34.4$ nm and $c = 21.3$ nm [12].

It should be noted that the observed small angle XRD pattern agrees well with the expected relative peak positions for a 3D-HPL structure as summarized in Table 4. To describe the detailed supramolecular structure of HPL mesophase, it is useful to calculate the number of molecules per unit cell.

There are four layers of rod block in unit cell. The density of rod block in mesophase can be calculated using specific thermal expansivity of PET, and that of melted PE and PEO blocks in mesophase can be calculated by specific thermal expansivity of amorphous ones. From calculation [13] based on

the lattice parameters of the 3D unit cell and calculated density, monomer and dimer have approximately 3160 and 2320 rod molecules per a single layer of rod block in each unit cell. On the basis of the calculated density and length of rod segments [14], perforation diameters ($d = 2r$) of monomer and dimer can be calculated 26.7 and 23.4 nm, with wall thickness ($W$) of 13.0 and 11.0 nm, in a single layer of rod block (Fig. 9).

The supramolecular structure can be described as a honeycomblike liquid crystalline layer of rod segments with in-plane hexagonal packing of PE coil perforations [15]. The consequent layers are stacked in AB–BA arrangement to generate a 3D order. The perforation can be considered as a dislike cylinder since the stiff rod segments are aligned axially with respect to the layer normal. The coil-rod-coil ABC triblock molecular architecture is comprised of a hydrophobic flexible coil A block, a hydrophobic stiff rod B block, and a hydrophilic flexible coil C blocks, which drives microphase
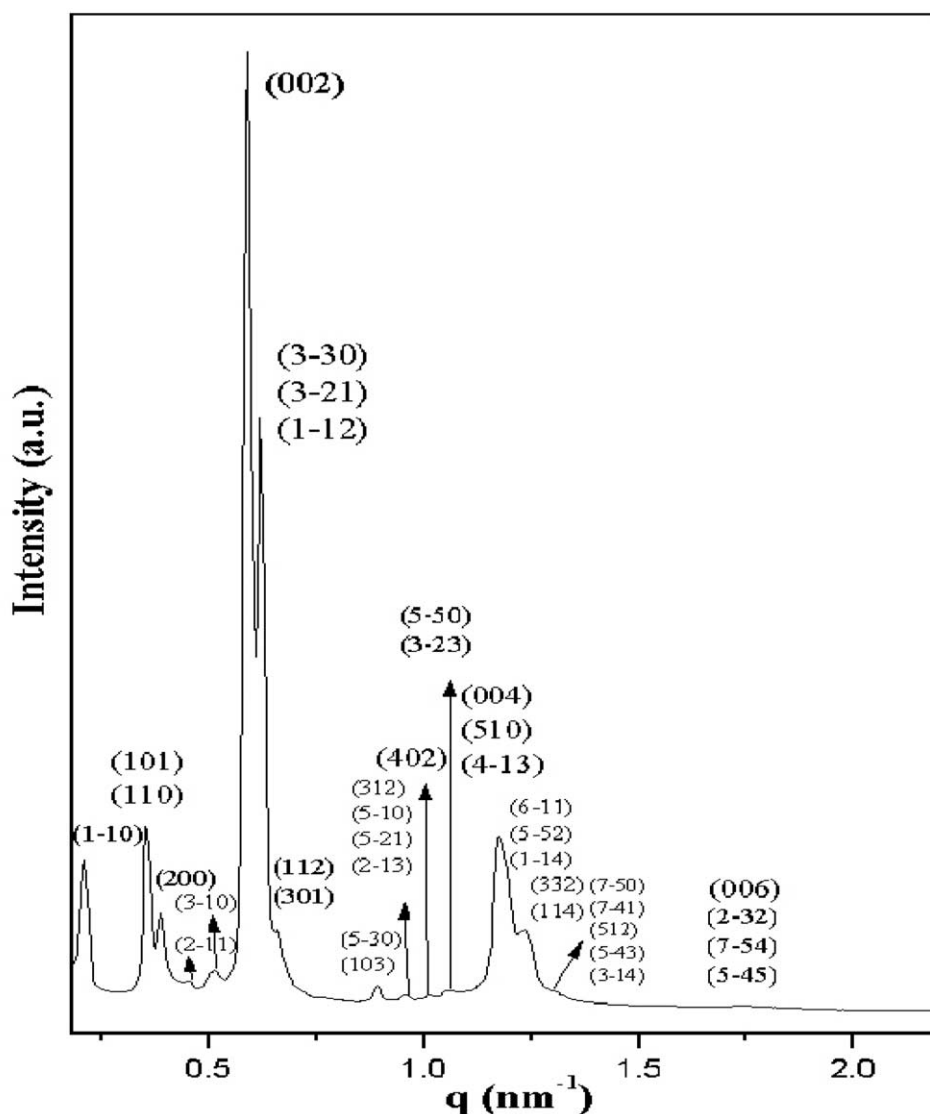


Fig. 8. Small angle XRD pattern of dimer measured at 117 °C.

Table 4
Small angle XRD data for hexagonally perforated lamellar structure of dimer

| h k l | $q_{obsd}$ (nm$^{-1}$) | $q_{calcd}$ (nm$^{-1}$) |
|---|---|---|
| 1 −1 0 | 0.214 | 0.214 |
| 1 0 1 | 0.358 | 0.363 |
| 1 1 0 | 0.358 | 0.363 |
| 2 0 0 | 0.388 | 0.420 |
| 2 −1 −1 | 0.457 | 0.470 |
| 3 −1 0 | 0.518 | 0.555 |
| 0 0 2 | 0.591 | 0.591 |
| 3 −3 0 | 0.627 | 0.627 |
| 3 −2 1 | 0.627 | 0.627 |
| 1 −1 2 | 0.627 | 0.627 |
| 1 1 2 | 0.660 | 0.698 |
| 3 0 1 | 0.660 | 0.698 |
| 5 −3 0 | 0.897 | 0.911 |
| 1 0 3 | 0.897 | 0.911 |
| 3 1 2 | 0.958 | 0.961 |
| 5 −1 0 | 0.958 | 0.961 |
| 5 −2 1 | 0.958 | 0.961 |
| 2 −1 3 | 0.958 | 0.961 |
| 4 0 2 | 1.018 | 1.033 |
| 5 −5 0 | 1.057 | 1.047 |
| 3 −2 3 | 1.057 | 1.047 |
| 0 0 4 | 1.168 | 1.168 |
| 5 1 0 | 1.168 | 1.168 |
| 4 −1 3 | 1.168 | 1.168 |
| 6 −1 1 | 1.195 | 1.203 |
| 5 −5 2 | 1.195 | 1.203 |
| 1 −1 4 | 1.195 | 1.203 |
| 3 3 2 | 1.237 | 1.239 |
| 1 1 4 | 1.237 | 1.239 |
| 7 −5 0 | 1.310 | 1.310 |
| 7 −4 1 | 1.310 | 1.310 |
| 5 1 2 | 1.310 | 1.310 |
| 5 −4 3 | 1.310 | 1.310 |
| 3 −1 4 | 1.310 | 1.310 |
| 0 0 6 | 1.743 | 1.766 |
| 2 −3 2 | 1.743 | 1.766 |
| 7 −5 4 | 1.743 | 1.766 |
| 5 −4 5 | 1.743 | 1.766 |

$q_{obsd}$ and $q_{calcd}$ are the scattering vectors of the observed reflections (Fig. 8) and calculated for the hexagonally perforated lamellar structure (P6$_3$/mmc space group symmetry) with lattice parameters $a = 34.4$ nm and $c = 21.3$ nm.



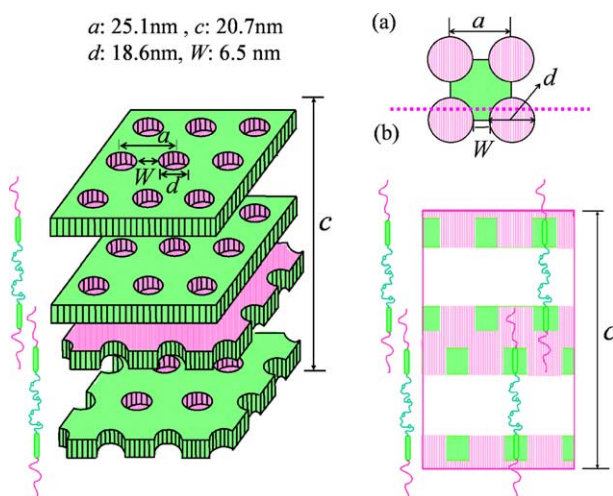a: 25.1nm, c: 20.7nm
d: 18.6nm, W: 6.5 nm

Fig. 9. Schematic representation of 3D hexagonally perforated lamellar (P6$_3$/mmc space group symmetry) structure of monomer and dimer.

separation into alternating layers of a hydrophobic PE and rod blocks and a hydrophilic PEO blocks due to large chemical differences between each block.

However, the lamellar ordering of rods would confine coil-rod-coil junctions to a flat interface with a relatively high density of grafting sites. To minimize coil deformation and fill space efficiently, splaying hydrophobic PE chains perforated into lamellar hydrophobic rod-domains. The lattice parameter $c$ of HPL mesophase in dimer is similar to that of monomer. The perforated lamellar mesophase of triblock molecules is self-assembled by a constant $C$ coil volume fraction. However, lattice parameter $a$, which is the distance between perforated PE blocks, of HPL mesophase in dimer is shorter than that of monomer due to the restriction effect of chain end mobility. Dimer has a tendency to self-assemble further well-defined HPL mesophase compared with monomer.

At 126 °C, the small angle XRD pattern of dimer shows two sharp and weak reflections as shown in Fig. 4(b), which can be indexed as 3D tetragonally perforated lamellar (TPL) mesophase with lattice parameters $a = 25.1$ nm and $c = 20.7$ nm (Table 5).

TPL structures have been observed in the intermediate phase called 'T phase' between lamellar and columnar phases of surfactant molecules [16]. To describe the TPL mesophase suprmolecular structure in detail, it is useful to calculate the number of molecules per unit cell. Based on the lattice parameters of the 3D unit cell and calculated density, dimer is calculated to have approximately 1390 rod molecules per a single layer of rod block in each unit cell [17]. On the basis of the calculated density and length of rod segment [18], perforation diameter ($d$) and wall thickness ($W$) of dimer are 18.6 and 6.5 nm in a single layer of rod block (Fig. 10).

In comparison with HPL structure, the lattice parameter $c$ of TPL structure slightly decreases while lattice parameter $a$ decreases considerably. By increasing temperature (from HPL to TPL), the distance between rod layers of perforation lamellar structure does not change noticeably, and perforated PE chains in the rod segment self-assemble from a hexagonal to tetragonal array. Compared to monomer, dimer has a tendency to self-assemble from HPL to TPL mesophase, most probably due to the restriction effect of chain end mobility.

At 132 °C, dimer exhibits hexagonal columnar mesophase, showing characteristic pseudo-focal conic textures confirmed by POM observation. The small angle XRD pattern of dimer measured at a birefringent mesophase exhibits three sharp

Table 5
Small angle XRD data for tetragonally perforated lamellar structure of dimer

| h k l | $q_{obsd}$ (nm$^{-1}$) | $q_{calcd}$ (nm$^{-1}$) |
|---|---|---|
| 1 1 0 | 0.356 | 0.356 |
| 1 0 1 | 0.388 | 0.388 |
| 0 0 2 | 0.6.8 | 0.608 |
| 0 0 4 | 1.216 | 1.216 |

$q_{obsd}$ and $q_{calcd}$ are the scattering vectors of the observed reflections (at 126 °C in Fig. 4(b)) and calculated for the tetragonally perforated lamellar structure (14/mmm space group symmetry) with lattice parameters $a = 25.1$ nm and $c = 20.7$ nm.
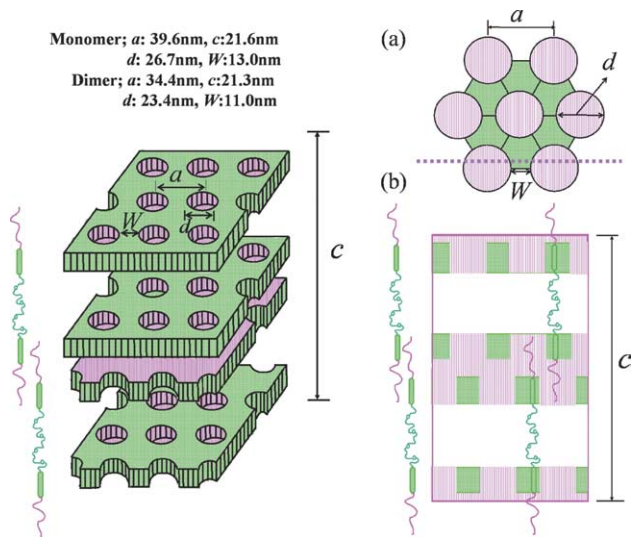
Fig. 10. Schematic representation of 3D tetragonally perforated lamellar (*I4/mmm* space group symmetry) structure of dimer.

reflections with the ratio of 1:$\sqrt{3}$:2 (Fig. 4(b)). This can be indexed as 2D hexagonal columnar mesophase with a lattice parameter of $a = 11.3$ nm. Even though small angle XRD pattern of monomer exhibits two sharp reflections with the ratio of 1:2 (Fig. 4(a)), it is considered to be hexagonal columnar mesophase. These results indicate that the order of dimer in hexagonal columnar mesophase showed further well-defined supramolecular structure than that of monomer. To describe the detailed supramolecular structure of the 2D hexagonal columnar mesophase, it is useful to calculate the number of molecules per cross-sectional slice of a column. Based on the lattice parameter of the unit cell and calculated density, the

average number ($n$) of rod molecules of monomer and dimer is approximately 14 and 12 per cross-section of a cylinder [19].

The inner core of the cylinder is composed of PE chains and two discrete rod segment cores with a rectangular cross-section, while PEO chains fill the outer intercylinder matrix.

Dimer exhibits enantiotropic optically isotropic mesophase at 135 °C. The small angle XRD measurement in an optically isotropic state revealed a strong primary peak together with a broad peak of weak intensity at about 1.8 relative to the primary peak position [4], [20]. This indicates that optically isotropic phase is a discrete spherical micellar mesophase with a lack of cubic symmetry.

Assuming liquidlike spherical micelles, an approximate diameter ($d$) of the sphere was calculated from $d = 1.23(2\pi/q)$, where $q$ is a scattering vector obtained from the primary peak of the small angle XRD pattern measured at optically isotropic phase [21]. To describe the detailed supramolecular structure of spherical micellar mesophase, it is desirable to calculate the number of rod molecules per micelle. Based on sphere diameter and calculated density, dimer has approximately 165 molecules in each micelle [22]. The aggregation of approximately 330 rod segments in a micelle is estimated to give rise to a supramolecular rod bundle with two hockey puck-like cylinder shapes, considering that the rod bundles are aligned randomly. On the basis of these results, the schematic representation for the inner core of the micelle can construct PE chains and two discrete rod segment cores, while PEO chains fill the outer intermicellar matrix [4].

The spherical micellar supramolecular structure is believed to originate from the anisotropic orientation of rods within microphase-separated aromatic domains and resulting entropic penalties associated with PEO chain stretching.
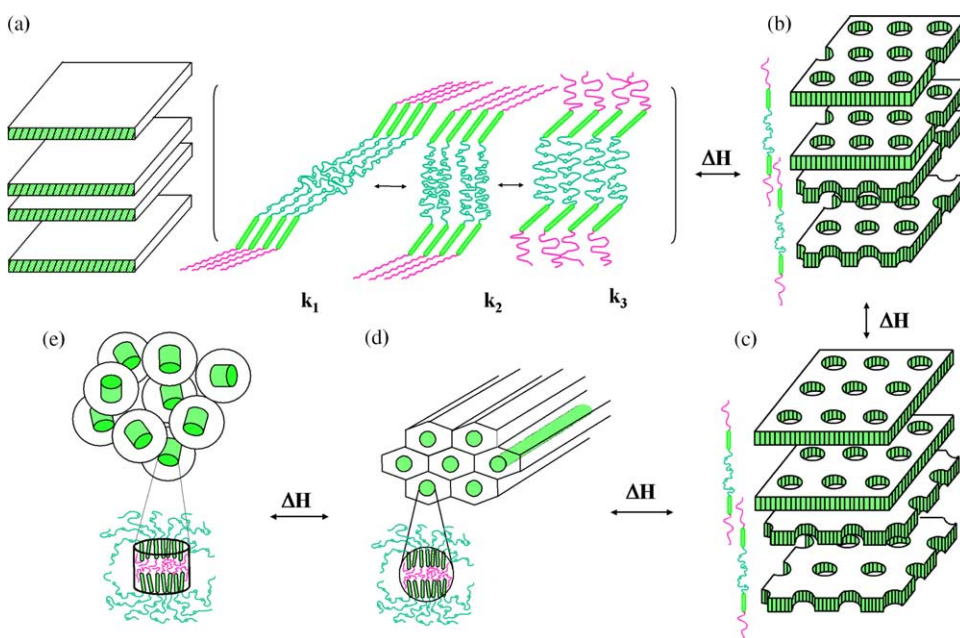


Fig. 11. Schematic representation of self-assemblies of dimer molecule in (a) lamellar crystalline phase and (b) hexagonally perforated lamellar (HPL), (c) tetragonally perforated lamellar (TPL), (d) hexagonal columnar (Col), and (e) spherical micellar (M) liquid crystalline phases.

Consequently, the molecular organization of rods in each spherical micelle favoring anisotropic orientation with their long axes would give rise to micellar cores with cylindrical-shape rather than spherical-shape. In comparison with monomer, dimer has a tendency to self-assemble into spherical micellar mesophase by simple binding of coil block. These results suggest that our approach to control supramolcular structures can be controlled by slight restriction of chain end mobility.

## 4. Conclusion

The coil-rod-coil ABC triblock (monomer) and coil-rod-coil-rod-coil ABCBA triblock dimer (dimer) molecules were synthesized and their self-assembling behavior in solid and melt states were investigated. In crystalline phase, monomer and dimer exhibited three different crystalline melting transitions associated with PEO, PE, and rod blocks, respectively. In comparison with monomer, dimer has a tendency to self-assemble into various well-defined supra-molecular nanostructures in liquid crystalline phases upon binding C coil block through covalent linkage. We present here the structural change of dimer in comparison with monomer, from lamellar crystalline phases to spherical micellar liquid crystalline (M) phase via hexagonally perforated lamellar (HPL), tetragonally perforated lamellar (TPL), and hexagonal columnar liquid crystalline (col) phase upon binding coil block (Fig. 11). Interestingly, dimer self-assembles from HPL to TPL mesophase due to restriction of chain end mobility, whereas, in monomer, only HPL mesophase is observed. These results suggest that we can control the supramolecular nanostructures through simple binding coil block.

## Acknowledgements

## References

[1] (a) Lee M, Cho BK, Zin WC. Chem Rev 2001;101:3869.
　　(b) Hamley IW. Angew Chem Int Ed 2003;42:1692.
　　(c) Ikkala O, Gerrit TB. Science 2002;295:2407.
　　(d) Park C, Yoon J, Thomas EL. Polymer 2003;44:6725.
　　(e) Nicol E, Niepceron F, Bonnans-Plaisance C, Durand D. Polymer 2005;46:2020.
　　(f) Triftaridou AI, Vamvakaki M, Patrickios CS. Polymer 2004;43:2921.
[2] (a) Radzilowski LH, Stupp SI. Macromolecules 1994;27:7747.
　　(b) Radzilowski LH, Carragher BO, Stupp SI. Macromolecules 1997;30:2110.
　　(c) Chen JT, Thomas EL, Ober CK, Mao GP. Science 1996;273:343.
　　(d) Stupp SI, LeBonheur V, Walker K, Li LS, Huggins KE, Kesser M, et al. Science 1997;276:384.
　　(e) Sleytr UB, Messner P, Pum D, Sara M. Angew Chem Int Ed 1999;38:1034.
　　(f) Oesterbacka R, An CP, Jiang XM, Vardeny ZV. Science 2000;287:839.
　　(g) Jenekhe SA, Chen XL. Science 1999;283:372.
　　(h) Chen B, Baumeister U, Das MK, Zeng X, Ungar G, Tschierske C. J Am Chem Soc 2004;126:8608.
　　(i) Minich EA, Nowak AP, Deming TJ, Pochan DJ. Polymer 2004;45:1951.
　　(j) Chen ZR, Kornfield JA. Polymer 1998;39:4679.
[3] (a) Stupp SI, Braun PV. Science 1997;277:1242.
　　(b) Kato T. Science 2002;295:2414.
　　(c) Yoshio M, Mukai T, Kanie K, Yoshizawa M, Ohno H, Kato T. Adv Mater 2002;14:351.
　　(d) Percec V, Glodde M, Bera TK, Miura Y, Shiyanovskaya I, Singer KD, et al. Nature 2002;419:384.
　　(e) Lee M, Jeong YS, Cho BK, Oh NK, Zin WC. Chem Eur J 2002;8:876.
　　(f) de Boer B, Stalmach Ulf, van Hutten PF, Melzer C, Krasnikov VV, Hadziioannou G. Polymer 2001;42:9097.
　　(g) Imanishi Y, Kimura S. Polymer 1996;37:4929.
[4] Lee M, Lee DW, Cho BK, Yoon JY, Zin WC. J Am Chem Soc 1998;120:13258.
[5] Oh NK, Zin WC, Im JH, Ryu JH, Lee M. Chem Commun 2004;1092.
[6] Lee M, Oh KN. J Mater Chem 1996;6:1079.
[7] Percec V, Lee M. Macromolecules 1992;24:2780.
[8] Kavesh SR, Schultz JM. J Polym Sci 1970;8:243.
[9] Takahashi Y, Tadokoro H. Macromolecules 1973;6:672.
[10] Destrade C, Foucher P, Gasparoux HT. Mol Cryst Liq Cryst 1984;106:121.
[11] Hareng M, Le Berre S, Lab C, Rech T, Orsay F. J Phys Colloque 1976;3:135.
[12] (a) Qi S, Wang ZG. Macromolecules 1997;30:4491.
　　(b) Ahn JH, Zin WC. Macromolecules 2000;33:641.
　　(c) Forser S, Khandpur AK, Zhao J, Bates FS, Hamley IW, Ryan AJ, et al. Macromolecules 1994;27:6922.

[13] From the lattice parameters ($a$ and $c$) and calculated density, the average number ($n$) of rod molecules arranged in a single layer of rod block of unit cell can be calculated according to Eq. (1), where $M$ is the molecular weight and $N_A$ is Avogadro's number.

$$4n = \left(\frac{\sqrt{3}}{2}\right)a^2 c\left(\frac{N_A\rho}{M}\right) \tag{1}$$

[14] The perforation diameter of coil in a single layer of rod block can be calculated according to Eq. (2), from perforated coil volume ($V_{pc}$), where $\rho_{rod}$ is density of rod segment, and $h = 21.6$ Å (estimated using Material Studio Software) is the length of the rod segment.

$$\pi r^2 h = \frac{\sqrt{3}}{2}a^2 h - \frac{nM_{rod}}{N_A\rho_{rod}} = V_{pc} \tag{2}$$

[15] Chen B, Zeng XB, Baumeister U, Diele S, Ungar G, Tschierske C. Angew Chem Int Ed 2004;43:4621.
[16] (a) Luzzati V, Tardieu A, Gulik-Krzwichi T. Nature 1968;217:1028.
　　(b) Luzzati V, Vargas R, Gulik A, Mariani P, Seddon JM, Rivas E. Biochemistry 1992;31:279.

[17] The average number ($n$) of rod molecules arranged in a single layer of rod block of unit cell can be calculated according to Eq. (3), from the lattice parameters ($a$ and $c$) and calculated density.

$$4n = a^2 c\left(\frac{N_A\rho}{M}\right) \tag{3}$$

[18] From perforated coil volume ($V_{pc}$) in a single rod layer, the perforation diameter ($d=2r$) of coil can be calculated according to Eq. (4)

$$\pi r^2 h = a^2 h - \frac{n M_{rod}}{N_A \rho_{rod}} = V_{pc} \qquad (4)$$

[19] From the experimental values of the intercolumnar distance ($a$) and density ($\rho$), the average number ($n$) of rod molecules arranged side by side in a single slice of cylinders with thickness ($t$) can be calculated according to Eq. (5), where $t$ is estimated 5.1 Å to be by the length and density of the rod block.

$$n = \left(\frac{\sqrt{3}}{2}\right) a^2 t \left(\frac{N_A \rho}{M}\right) \qquad (5)$$

[20] Guinier A. X-ray diffraction. San Francisco, CA: W.H. Freeman and Co.; 1963.

[21] (a) Sakamoto M, Hashimoto T, Han CD, Vaidya NY. Macromolecules 1997;30:1621.
     (b) Schwab M, Stuehn B. Phys Rev Lett 1996;76:924.

[22] From the diameter ($d$) of sphere and calculated density, the average number ($n$) of dimer in the sphere can be estimated according to Eq. (6).

$$n = \frac{4}{3}\pi \left(\frac{d}{2}\right)^3 \left(\frac{N_A \rho}{M}\right) \qquad (6)$$